

# Localized Basis for Effective Lattice Hamiltonians: Lattice Wannier Functions

K. M. Rabe and U. V. Waghmare

*Yale University, Department of Applied Physics*

*P. O. Box 208284, New Haven, Connecticut, 06520-8284*

## Abstract

A systematic method is presented for constructing effective Hamiltonians for general phonon-related structural transitions. The key feature is the application of group theoretical methods to identify the subspace in which the effective Hamiltonian acts and construct for it localized basis vectors, which are the analogue of electronic Wannier functions. The results of the symmetry analysis for the perovskite, rocksalt, fluorite and A15 structures and the forms of effective Hamiltonians for the ferroelectric transition in  $PbTiO_3$  and  $BaTiO_3$ , the oxygen-octahedron rotation transition in  $SrTiO_3$ , the Jahn-Teller instability in  $La_{1-x}(Ca, Sr, Ba)_xMnO_3$  and the antiferroelectric transition in  $PbZrO_3$  are discussed. For the oxygen-octahedron rotation transition in  $SrTiO_3$ , this method provides an alternative to the rotational variable approach which is well behaved throughout the Brillouin zone. The parameters appearing in the Wannier basis vectors and in the effective Hamiltonian, given by the corresponding invariant energy expansion, can be obtained for individual materials using first-principles density-functional-theory total energy and linear response techniques, or any technique that can reliably calculate force constants and distortion energies. A practical approach to the determination of these parameters is presented and the application to ferroelectric  $PbTiO_3$

arXiv:mr1-th/9411006v2 27 Aug 1995

discussed.

63.75.+z, 63.20.Dj, 61.50.Em, 77.80.Bh

## I. INTRODUCTION

Interest in the construction of effective Hamiltonians to relate macroscopic properties of materials to microscopic information has recently increased dramatically. Construction of an effective lattice Hamiltonian is greatly facilitated by the use of a localized basis for the description of crystal structure distortions. For example, structural phase transitions in perovskite and rocksalt structure systems have been studied using model Hamiltonians with a “local mode” basis to describe the unstable lattice modes relevant to the transition. While in earlier work the microscopic model parameters had to be determined empirically,<sup>1–3</sup> recent advances in the accuracy and efficiency of first-principles bandstructure and total energy methods have made it possible to calculate these parameters directly from first principles, and encouraging agreement with experimentally observed transition properties has been obtained.<sup>4–7</sup> In addition, the study of electronic properties of systems which exhibit lattice instabilities coupled to the electronic states is facilitated by the description of the lattice in a localized basis, putting it on an equal footing with the usual tight-binding description of the electronic states.<sup>8</sup> However, the approximate “local mode” basis is expected to be inadequate for high-accuracy first-principles investigations. Furthermore, explicit construction of a localized basis set and optimal effective Hamiltonian has proved to be especially problematic for complicated crystal structures and structural transitions involving modes at the zone boundary or interior of the zone.

In this paper, we present a systematic procedure for the construction of an effective lattice Hamiltonian in a localized basis set, applicable to arbitrary systems and structures and specifically designed for practical use in first-principles studies. This approach is suitable for the investigation of a general phonon-related structural transition,<sup>9</sup> involving a small change in structure which can be generated by freezing phonon displacements into a high-symmetry prototype structure. We implement this procedure for structural transitions in the perovskite, rocksalt, fluorite and A15 structures. Group theoretical methods, which since Landau<sup>10</sup> have been central to the phenomenological study of structural phase transitions,

are essential to our development of a procedure which is systematic and easy to implement for arbitrary structures and transitions. The resulting localized basis vectors are the lattice analogue<sup>1,2,11,12</sup> of electronic Wannier functions.<sup>13,14</sup> These Wannier basis vectors span an invariant subspace containing the low-frequency normal modes relevant to the transition. This subspace is energetically decoupled at quadratic order from the higher frequency eigenmodes, permitting the construction of an effective Hamiltonian for the transition including only lattice distortions in the subspace. The model parameters for a particular material can be obtained using any method that can reliably calculate force constants and distortion energies. For the force constant calculation, the most efficient high-accuracy method is density-functional-theory (DFT) linear response.<sup>15–18</sup> As we will see, once the force-constant matrices have been calculated, an effective Hamiltonian can be constructed with very little additional effort. The final result is a model system which reproduces the finite-temperature transition behavior of the original lattice Hamiltonian, while the simpler form and reduction in the number of degrees of freedom per unit cell make it suitable for study by methods such as mean field theory and Monte Carlo simulation.

In the next section, we present the derivation of the effective Hamiltonian in a symmetrized localized (Wannier) basis. In Section III, we discuss in detail the construction of the Wannier basis and resulting effective Hamiltonian for the simple example of the diatomic chain. In Section IV, this construction is generalized to arbitrary structures and applied to the structural transitions in perovskite compounds. In addition, the results of the construction for the rocksalt, fluorite and A15 structures are briefly described. Section V is a discussion of the practical implementation of this approach in a first-principles framework, illustrated by application to the ferroelectric transition in *PbTiO<sub>3</sub>*. Finally, Section VI summarizes and concludes the paper.

## II. FORMAL DERIVATION OF THE EFFECTIVE HAMILTONIAN

Consider a crystal with  $n_{at}$  atoms per unit cell and  $N$  unit cells with Born-von Karman boundary conditions. Each possible configuration of the crystal is fully described by specifying the generalized displacement of each ion (i.e. the displacement multiplied by the square root of the ion mass) relative to a fixed high-symmetry reference structure, which should be chosen so that the physically important configurations are obtained by small distortions. In general, this will be the same as the structure of the high-symmetry phase. The set of all ionic displacement patterns forms a  $3n_{at}N$ -dimensional vector space, called the “ionic-displacement space.” In the standard basis, in which each basis vector is the unit displacement of a single ion in a single cartesian direction, the coordinates of a particular configuration are the generalized displacements  $\{u_{j\alpha}, j = 1, n_{at}N; \alpha = x, y, z\}$ . Another basis for the ionic-displacement space is obtained from the normal modes  $\{e_{\vec{k}\lambda}; \vec{k} \in \text{Brillouin zone}, \lambda = 1, 3n_{at}\}$ . In this basis, the coordinates  $\{c_{\vec{k}\lambda}\}$  are complex numbers, with the understanding that the ionic-displacement pattern is obtained by taking the real part of the vector  $\sum_{\vec{k}, \lambda} c_{\vec{k}\lambda} e_{\vec{k}\lambda}$ . The  $\{e_{\vec{k}\lambda}\}$  transform according to irreducible representations of the space group of the high-symmetry reference structure  $\mathcal{G}_0$ . For example, the action of translation through a lattice vector is  $\mathcal{O}_{\vec{R}} e_{\vec{k}\lambda} = \exp(i\vec{k} \cdot \vec{R}) e_{\vec{k}\lambda}$ .

For the construction of an effective Hamiltonian, we perform a decomposition of the ionic-displacement space into invariant subspaces, called “band subspaces,” spanned by one or more entire branches of the normal modes and closed under  $\mathcal{G}_0$ <sup>14</sup> Each band subspace in this decomposition should be minimal in the sense that it cannot be written as the direct sum of two band subspaces. The number of band subspaces is  $n_s$  and they are indexed by  $\Lambda$ , with the number of branches in each subspace  $n_\Lambda$ , indexed by  $l$  (note that  $\sum_{\Lambda=1, n_s} n_\Lambda = 3n_{at}$ ).  $n_\Lambda$  will also be referred to as the multiplicity of the band subspace.

For each band subspace  $\Lambda$ , we seek a localized basis set with definite symmetry properties with respect to  $\mathcal{G}_0$ . These properties are established by choosing a Wyckoff symbol for  $\mathcal{G}_0$ , of multiplicity  $n_w$ , and an  $l_s$ -dimensional irreducible representation (irrep) of the corresponding

site symmetry group.<sup>14,19,20</sup> The choice of Wyckoff symbol and site symmetry group irrep is constrained by the requirement that the representation of  $\mathcal{G}_0$  defined by the localized basis have the same decomposition into irreps of  $\mathcal{G}_0$  as the particular band subspace  $\Lambda$  for which a basis is being sought. Specifically, a set of basis vectors  $\{w_{\Lambda ij\vec{R}_n}; j = 1, l_s\}$  is associated with a particular site in the crystal (the  $i$ th Wyckoff position added to the lattice vector  $\vec{R}_n$ ) and is a set of partner functions of the chosen irrep of the site symmetry group. These basis vectors are localized, with ionic displacements decaying rapidly with distance from the associated site. The basis vectors associated with the other sites of the chosen type are generated by acting on the given basis vectors with symmetry operations from  $\mathcal{G}_0$ . For example, subsets of localized basis vectors are related to each other by translation through a lattice vector  $w_{\Lambda ij\vec{R}_n+\vec{R}} = \mathcal{O}_{\vec{R}} w_{\Lambda ij\vec{R}_n}$ . Clearly, the product of the number of Wyckoff positions  $n_w$  and the dimension of the site symmetry group irrep  $l_s$  must equal the multiplicity of the band subspace  $n_\Lambda$ , and we replace the former two indices by a combined index  $l = 1, n_\Lambda$ . The decomposition of the localized basis representation of  $\mathcal{G}_0$  into irreps of  $\mathcal{G}_0$  can be computed from formulas such as Equation 14 in Ref. 19 or by computing, for various  $\vec{k}$ , the character table of  $\mathcal{G}_{\vec{k}}$  in the subspace of Bloch sums. Usually, the appropriate choice of Wyckoff symbol and site symmetry group irrep can be determined just from the space group irrep labels of the eigenmodes at the high-symmetry points.

The basis vectors from each band subspace in the decomposition can be combined to form a basis for the full ionic displacement space. In this basis, the coordinates of a particular configuration are the real numbers  $\{\xi_{\Lambda l i}; \Lambda = 1, n_s; l = 1, n_\Lambda; i = 1, N\}$ , which determine the ionic-displacement pattern as the vector  $\sum_{\Lambda l i} \xi_{\Lambda l i} w_{\Lambda l i}$ . These localized basis vectors are the lattice analogue<sup>1,2,11,12</sup> of electronic Wannier functions.<sup>13,14</sup> The symmetry properties of the Wannier basis vectors lead to a convenient form for the Taylor expansion of the lattice energy in the corresponding coordinates, allowing easy identification of independent parameters. Furthermore, the expansion has the important feature that it contains no quadratic cross terms between different band subspaces. Extra considerations apply when the various branches of normal modes include some with polar character and/or are not well

separated in energy; these will be discussed in Section V.

With this basis set, the derivation of an effective Hamiltonian proceeds as follows. The classical partition function for the lattice is:

$$Z \propto \int \{du_{j\alpha}\} \exp(-\beta \mathcal{H}_{lat}(\{u_{j\alpha}\})) \quad (2.1)$$

where  $j$  runs over the  $n_{at}N$  atoms, the electron degrees of freedom have been eliminated through the Born-Oppenheimer approximation, and the generalized ionic displacements  $\{u_{j\alpha}\}$  are measured relative to a high symmetry reference structure, as described above. The momentum integral leads to a trivial  $u$ -independent factor and is not explicitly written here.

It is straightforward to change variables in  $\mathcal{H}_{lat}$  from standard basis coordinates  $\{u_{j\alpha}\}$  to Wannier basis coordinates  $\{\xi_{\Lambda\vec{R}_i}\}$  and Taylor expand  $\mathcal{H}_{lat}$  around the reference structure. By construction, the quadratic part  $\mathcal{H}_{lat}^{(2)}$  decouples into a sum over the band subspaces:

$$\mathcal{H}_{lat}^{(2)}(\{\xi_{\Lambda\vec{R}_i}\}) = \sum_{\Lambda=1, n_s} \mathcal{H}_{\Lambda}^{(2)}(\{\xi_{\Lambda\vec{R}_i}\})$$

where

$$\mathcal{H}_{\Lambda}^{(2)}(\{\xi_{\Lambda\vec{R}_i}\}) = \sum_{l,l'=1, n_{\Lambda}} \sum_{i,j=1, N} a_{ll'j}^{(\Lambda)} \xi_{\Lambda\vec{R}_i} \xi_{\Lambda'\vec{R}_j}.$$

The next step is to choose a band subspace or direct sum of band subspaces as the symmetry-invariant subspace in which the effective Hamiltonian will act. This subspace should be as small as possible, yet should include all modes which have higher-order terms in the expansion of  $H_{lat}$  which are important in describing low-energy configurations, and which therefore cannot to a good approximation be dropped from the expansion in the evaluation of the partition function near the transition. For the calculation of thermodynamic behavior at temperatures in the vicinity of the structural transition, it is essential to include higher order terms for the branches containing the unstable modes associated with the transition. Strain degrees of freedom may not have important anharmonicity in themselves, but still have physically important higher-order coupling to the unstable modes, and thus should be considered for inclusion in the subspace. Here and in the rest of this section, we write the

expressions for the case that the effective Hamiltonian acts in a single band subspace  $\Lambda_0$ , since generalization to the case of the direct sum  $\Lambda_1 \oplus \Lambda_2 \oplus \dots \oplus \Lambda_s$  is straightforward. The correct choice of subspace permits the following approximation to  $H_{lat}$ :

$$\mathcal{H}_{lat} \approx \mathcal{H}_{eff}(\{\xi_{\Lambda_0 l \vec{R}_i}\}) + \sum_{\Lambda \neq \Lambda_0} \mathcal{H}_{\Lambda}^{(2)}(\{\xi_{\Lambda l \vec{R}_i}\}) \quad (2.2)$$

Within this approximation, anharmonic terms appear *only* in  $\mathcal{H}_{eff}$  and, by construction, there are *no* cross terms between  $\Lambda_0$  and  $\Lambda \neq \Lambda_0$ . This has the important consequence that the integration over the degrees of freedom not included in the effective Hamiltonian subspace can be performed analytically. Specifically, the partition function integral factorizes into an integral over  $\Lambda_0$  and another over  $\Lambda \neq \Lambda_0$ . The integral over  $\Lambda \neq \Lambda_0$  is an elementary Gaussian integral which leads to a temperature-dependent factor unimportant for the structural transition. The remaining integral has the form of a partition function for a system of  $n_{\Lambda_0}$ -component spins on a lattice  $\{\vec{R}_i\}$ , which recovers the original partition function  $Z$ :

$$\int \{d\xi_{\Lambda_0 l \vec{R}_i}\} \exp(-\beta \mathcal{H}_{eff}(\{\xi_{\Lambda_0 l \vec{R}_i}\})) \propto Z. \quad (2.3)$$

An explicit expression for  $\mathcal{H}_{eff}$  is obtained by making a Taylor expansion in symmetry invariant combinations of the  $\{\xi_{\Lambda_0 l \vec{R}_i}\}$ . This expansion is greatly facilitated by the symmetry properties of the Wannier basis. An expression with a finite number of undetermined parameters is obtained by setting expansion coefficients beyond a certain range or order to zero or writing them in a parametrized form. The resulting spin-like model is suitable for statistical mechanical analysis via mean field theory, Monte Carlo simulation, or other appropriate method. The values of the expansion coefficients are different for different materials and are to be obtained from first principles calculations, as will be discussed in Section V.

### III. EFFECTIVE HAMILTONIAN CONSTRUCTION: THE DIATOMIC CHAIN

In this section, the explicit construction of the effective Hamiltonian in a localized Wannier basis will be presented for the simple example of the diatomic chain.<sup>11</sup> This calcula-

tion demonstrates most, though not quite all, of the important principles, including the determination of the symmetry properties of the Wannier basis vectors. The remaining generalizations for application to arbitrary structures will be made in Section IV.

The high-symmetry reference structure of the “ionic” diatomic chain model we consider has lattice constant  $a = 1$  and ions A and B at positions  $n$  and  $n + \frac{1}{2}$  ( $n = 1, \dots, N$ ), respectively. The potential energy in our model is given to quadratic order in  $\{u_{nA}, u_{nB}\}$ , the displacements from the reference structure, by

$$\sum_n \left[ \frac{\alpha}{2} (u_{nB} - u_{nA})^2 + \frac{\alpha}{2} (u_{n-1,B} - u_{nA})^2 + \frac{\gamma}{2} (u_{n+1,B} - u_{nB})^2 \right] \quad (3.1)$$

as shown in Fig. 1. In the rest of this section, we set the masses of the ions  $m_A = m_B = 1$  and the ratio  $\frac{\gamma}{\alpha} = 0.25$ .

Analytical diagonalization of the dynamical matrix at each  $k$  in the first Brillouin zone yields two branches ( $\lambda = 1, 2$ ) with eigenvalues  $\epsilon_\Lambda(k) = \omega_\Lambda^2(k)$ , shown in Fig. 2. The normal modes are labelled by the irreps of the space group  $\{\{U|n\hat{x}\}, U = E, I; n = 1, \dots, N\}$ . These are  $\Gamma_g$  and  $\Gamma_u$  at  $k = 0$ ,  $X_g$  and  $X_u$  at  $k = \pi$ , and  $k$  otherwise. It can be seen that the ionic displacement space of the diatomic chain decomposes into two band subspaces  $\Lambda = 1, 2$ , each spanned by the nondegenerate eigenmode branch of corresponding  $\lambda$ . Since the number of branches in each subspace is one, we drop the index  $l$ .

As we have seen in Section II, construction of an effective Hamiltonian involves the choice of an invariant subspace. This subspace should be a band subspace (or direct sum of band subspaces) which includes all modes relevant to the particular transition being modelled. In the diatomic chain example, we imagine that the relevant mode is  $X_u$ . The band subspace  $\Lambda = 1$  has the symmetry label  $X_u$ , while the band subspace  $\Lambda = 2$  has the symmetry label  $X_g$ . Therefore, the subspace in which the effective Hamiltonian will act is  $\Lambda = 1$ . If instead the relevant mode were  $X_g$ , the corresponding effective Hamiltonian subspace would be  $\Lambda = 2$ .

For the chosen effective Hamiltonian subspace  $\Lambda = 1$  or  $\Lambda = 2$ , we seek a localized basis set labelled by a unit-multiplicity Wyckoff symbol and a one-dimensional irrep of the

corresponding site symmetry group, since both band subspaces are of unit multiplicity. The space group of the diatomic chain has two Wyckoff symbols of unit multiplicity:  $1a$ , (at  $x=0$ ), and  $1b$  (at  $x=1/2$ ). For both  $1a$  and  $1b$ , the site symmetry group is  $\bar{1}$ , with two one-dimensional irreps  $A_g$  (even) and  $A_u$  (odd). The space group representations defined by each of the four distinct labels  $(1a, A_g)$ ,  $(1a, A_u)$ ,  $(1b, A_g)$  and  $(1b, A_u)$  decompose at the high-symmetry k-points  $k = 0$  and  $k = \pi$  into the space group irreps  $(\Gamma_+, X_+)$ ,  $(\Gamma_-, X_-)$ ,  $(\Gamma_+, X_-)$ , and  $(\Gamma_-, X_+)$ , respectively. Since the space group irrep labels of the localized basis set must match those of the band subspace throughout the Brillouin zone, we find that for both band subspaces the label of the Wannier basis is uniquely determined. For  $\Lambda = 1$ , it is  $(1a, A_u)$ , and for  $\Lambda = 2$ , it is  $(1b, A_u)$ .

Since individual ionic displacements are a localized basis with the required symmetry properties for the full ionic displacement space, it might seem that the Wannier basis vectors would always be obtained from occupied Wyckoff positions combined with vector representations of the site symmetry group, as in the diatomic chain example. In fact, this is not the case. The simplest example in which this can be seen is the “molecular” diatomic chain.<sup>11</sup> For the present discussion, we consider the closely related triatomic chain model in Fig. 3. The high-symmetry reference structure has lattice constant  $a = 1$  and ions A at positions  $n$  and ions B at positions  $n \pm \frac{1}{3}$  ( $n = 1, \dots, N$ ). The space group is the same as that of the “ionic” diatomic chain discussed above. The space group irreps for the normal modes at the high-symmetry k-points are  $\Gamma_g$ ,  $\Gamma_u$ , and  $\Gamma_u$  at  $k = 0$  and  $X_g$ ,  $X_u$  and  $X_u$  at  $k = \pi$ . All space group irreps at the two points are compatible, so depending on the details of the potential, four types of branches defining unit-multiplicity band subspaces can appear. The Wannier basis of the band subspace  $(\Gamma_u, X_u)$  is labelled by  $(1a, A_u)$ , so that the basis vectors transform like ionic displacements at occupied Wyckoff positions. However, the Wannier basis of the band subspace  $(\Gamma_g, X_g)$  is labelled by  $(1a, A_g)$  and the Wannier bases of the two “mixed-label” band subspaces  $(\Gamma_u, X_g)$  and  $(\Gamma_g, X_u)$  are labelled by the unoccupied Wyckoff position  $1b$ , midway between the two B atoms, and the site symmetry group irreps  $A_u$  and  $A_g$ , respectively. For the triatomic chain, with an appropriate choice

of  $\alpha$  and  $\gamma$ , it may happen that there will be two band subspaces of the  $(\Gamma_u, X_u)$  type. Both will be described by Wannier basis vectors with labels  $(1a, A_u)$ , but the Wannier basis vectors for the two band subspaces will be orthogonal to each other.

For the complete construction of an effective Hamiltonian, it is not enough to know the symmetry properties of the basis vectors; rather, an explicit expression for the Wannier basis vectors in terms of ionic displacements is needed. The basis vectors are determined by the potential energy and resulting set of normal modes which define the band subspace. If the normal modes are known at all  $k$ , the basis vectors can be obtained exactly. For each  $\Lambda$ , the expression for  $w_{\Lambda n}$ , the Wannier basis vector centered in unit cell  $n$ , in terms of  $\{e_{k\Lambda}\}$  is

$$w_{\Lambda n} = \frac{1}{N} \sum_{-\pi < k \leq \pi} \exp(i\phi_{\Lambda}(k)) e_{k\Lambda} \exp(-ikn). \quad (3.2)$$

An inverse transform can be performed to express the  $\{e_{k\Lambda}\}$  in terms of the Wannier basis vectors:

$$e_{k\Lambda} = \exp(-i\phi_{\Lambda}(k)) \sum_n \exp(ikn) w_{\Lambda n}. \quad (3.3)$$

In evaluating Equation 3.2, the phase function  $\phi_{\Lambda}(k)$  can be freely chosen to maximize the localized character of  $w_{\Lambda n}$ , with the only constraint being the requirement that the resulting Wannier basis vectors have the desired symmetry properties. For the diatomic chain, the normal modes are easily obtained at all  $k$ . We follow the convention that the real part of the 2-component eigenvector  $(\Delta_{kA}^{(\lambda)}, \Delta_{kB}^{(\lambda)})$  of the 2x2 dynamical matrix at each  $k$  gives the displacements of the A and B ions in the unit cell  $n = 0$ . The displacements of the A and B ions in the unit cell  $n$  then are  $Re(\Delta_{kA}^{(\lambda)} \exp(ikn))$  and  $Re(\Delta_{kB}^{(\lambda)} \exp(ikn))$ .  $\Delta_{kA}^{(\lambda)}$  and  $\Delta_{kB}^{(\lambda)}$  can be chosen to satisfy  $|\Delta_{kA}^{(\lambda)}|^2 + |\Delta_{kB}^{(\lambda)}|^2 = 1$ ,  $\Delta_{kA}^{(\lambda)*} = \Delta_{-kA}^{(\lambda)}$  and  $\Delta_{kB}^{(\lambda)*} = \Delta_{-kB}^{(\lambda)}$  and to be smooth functions of  $k$ , ensuring that the corresponding normal mode  $e_{k\lambda}$  smoothly depends on  $k$ . For  $\Lambda = 1$ , we choose  $(\Delta_{kA}, \Delta_{kB})$  such that  $\Delta_{kA}$  is real and positive for all  $k$ , and  $\phi_{\Lambda}(k) = 0$ . The resulting Wannier basis vector  $w_{1n}$  is shown in Fig. 4.

Except in special cases such as the diatomic chain, knowledge of the normal modes at all  $k$  is not available and the expression in Equation 3.2 cannot be used to construct the

Wannier basis vectors. However, a good approximation can be obtained from knowledge of the eigenvectors at a subset of  $k$ -points through a fitting procedure which will prove to be practical for use with first-principles calculations. For a particular choice of Wyckoff symbol and site symmetry irrep, a parametrization of the displacement pattern of the Wannier basis vectors is obtained from symmetry considerations. For example, for the Wannier basis ( $1a, A_u$ ) of the  $\Lambda = 1$  subspace of the diatomic chain, the displacement of the central ion is given by one real parameter and each pair of ions equidistant from the center requires an additional real parameter to specify the equal displacements (see Fig. 4). The parameters of the Wannier basis vector, starting with the innermost coordination shells, are then fit to reproduce a set of known normal modes in the band subspace. Since the Wannier basis vector is localized, it should be a good approximation to set the displacement parameters to zero beyond a finite number of shells. For example, in the diatomic chain, the simplest nontrivial truncation is at the first shell. For  $\Lambda = 1$ , the fit to the eigenvector at  $k = 0$  yields the approximate Wannier basis vectors  $w_{1n}^{(0)}$  with displacements  $\frac{1}{\sqrt{2}}$  for the central A ion and  $\frac{1}{2\sqrt{2}}$  for the first shell of B ions. The frequencies corresponding to the approximate normal modes  $\sum_n \exp(ikn)w_{1n}^{(0)}$ , computed from Eqn. 3.1 and shown in Fig. 5, agree very well with the true frequencies if the nonorthonormality of the basis vectors is taken into account. With the inclusion of just one more shell of A ions in the approximate Wannier basis vector to fit the normalized eigenmode at  $k = \pi$  shown in Fig. 2, it is nearly indistinguishable from the exact Wannier basis vector on the scale of Fig. 4 and unit normalization to within a few percent is achieved throughout the Brillouin zone. This construction also illustrates the point that the choice of phases for the eigenmodes is important in producing a well-localized Wannier basis vector. In this case, if the normalized eigenmode at  $k = \pi$  were multiplied by  $-1$ , the approximate Wannier basis vector would have larger displacements on the first A coordination shell than on the central A ion.

Using the symmetry properties of the Wannier basis vectors, the form of the effective Hamiltonian can be written as an invariant expansion of the energy in the Wannier basis coordinates of the subspace. We now consider the diatomic chain with effective Hamilto-

nian subspace  $\Lambda = 1$ . Since these coordinates have the same transformation properties as individual ionic displacements of the A ions, the effective Hamiltonian parameters can be put into direct correspondence with the familiar force constants of the monoatomic chain or with tight-binding parameters for a system with one  $p$  orbital per unit cell. Truncating the expansion at fourth order in onsite terms and at quadratic order and second neighbor in intersite terms yields:

$$\mathcal{H}_{eff}(\{\xi_{\Lambda n}\}) = \sum_n [a_0 \xi_{\Lambda n}^2 + b_0 \xi_{\Lambda n}^4] + \sum_{n,n' \text{ s.t. } |n-n'| \leq 2} a_{|n-n'|} \xi_{\Lambda n} \xi_{\Lambda n'} \quad (3.4)$$

The small number of expansion coefficients in this effective Hamiltonian can be determined from total energy data for a particular choice of  $\alpha$  and  $\gamma$ . Specifically, once the subspace Wannier basis vectors  $\{w_{\Lambda n}\}$  have been determined, the values of the coordinates  $\{\xi_{\Lambda n}\}$  specify a unique ionic configuration.  $\mathcal{H}_{eff}(\{\xi_{\Lambda n}\})$  is then taken as the potential energy of this configuration. Calculation of the coefficients  $a_n$  in the invariant expansion proceeds by fitting the sum of quadratic terms in Equation 3.4 for coordinates  $\{\xi_{\Lambda n} = \text{Re}(\xi_k \exp(ikn))\}$ , at various  $k$ , to the quadratic energy of the corresponding ionic configurations, easily obtained from the dynamical matrix derived from Equation 3.1. For example, when  $\frac{\gamma}{\alpha} = 0.25$  the quadratic energy at  $k = 0$ ,  $k = \frac{\pi}{2}$  and  $k = \pi$  can be fit by  $a_0 = (13 - \sqrt{33})\alpha/16$ ,  $a_1 = -\alpha/4$  and  $a_2 = (-5 + \sqrt{33})\alpha/32$ . Comparison of the quadratic part of the effective Hamiltonian, truncated at  $a_2$ , with the true quadratic energy at other  $k$  is used to check the accuracy of the truncation of the invariant expansion, which in this case is within a few percent. Anharmonic parameters such as  $b_0$  are obtained from calculation and fitting of full potential energies for finite distortions.

In the study of structural transitions, focus on a simple description of a relevant mode at a particular k-point has occasionally led to a choice of localized basis vectors inconsistent with this symmetry criterion. As will be discussed in Section IV, a common example is the use of a rotational variable to describe the  $R_{25}$  instability in perovskites. The negative consequences of inconsistent symmetry can be simply illustrated in the diatomic chain. The displacement pattern of the  $X_g$  mode (Fig. 2) can be obtained with localized basis vectors

not only of the type  $(1b, A_u)$  but also  $(1a, A_g)$ , the latter being inconsistent with the symmetry criterion. As shown above, the choice of  $(1b, A_u)$  is the label of the Wannier basis for the  $\Lambda_2$  band subspace. However, localized basis vectors of the type  $(1a, A_g)$  lead to zero ionic displacements for  $k = 0$  distortions, showing that this “Wannier basis set” is in fact linearly dependent.

The problems encountered when using an inconsistent symmetry choice in the construction of the effective Hamiltonian can be understood using Equations 3.2 and 3.3. Wannier-like basis vectors inconsistent with our symmetry criterion can be constructed only if the requirement that the inverse transforms (Equation 3.3) reproduce *normalized* normal modes is lifted and zero normalization allowed. In Equation 3.2, this corresponds to multiplying the phase factor  $\exp(i\phi_\Lambda(k))$  by a real function  $f_\Lambda(k)$ . For example, Wannier-like functions of the type  $(1a, A_g)$  for the upper branch ( $\Lambda = 2$ ) can then be obtained with  $\phi_\Lambda(k) = \frac{\pi}{2}$  and  $f_\Lambda(k) = \frac{k}{\pi}$ . The inverse transforms reproduce the eigenmodes  $i\frac{k}{\pi}e_{k\Lambda}$ , not normalized to one except at  $k = \pi$ . The energy written in terms of the Fourier transform of the Wannier basis coordinates  $\xi_\Lambda(k) = \sum_n \exp(ikn)\xi_{\Lambda n}$  is

$$\sum_k \frac{k^2}{\pi^2} \epsilon_\Lambda(k) |\xi_\Lambda(k)|^2$$

Effective Hamiltonian parameters can be fit as above to reproduce the dispersion  $\frac{k^2}{\pi^2}\epsilon_\Lambda(k)$ . In particular, at  $k = 0$ , the parameters must be fit to zero energy. To use material-specific information at  $k = 0$ , it is necessary to expand the model dispersion to leading order in  $k^2$  and to fit the coefficient of  $\frac{k^2}{\pi^2}$  to  $\epsilon_\Lambda(k = 0)$ . The approximate Wannier basis vector construction can also be carried out as above except at  $k = 0$ , where it is necessary to expand the approximate eigenmode to leading order in  $k$  and to fit the coefficients to  $e_{k=0,\Lambda}$ . With  $f_\Lambda(k = 0) = 0$ , required to eliminate the inconsistent condition on the phases at  $k = 0$ , the resulting localized basis is linearly dependent and cannot reproduce the normal mode at  $k = 0$ . This amounts to eliminating the point  $k = 0$  from the ionic displacement space. In the thermodynamic limit, the behavior of the system should not be affected, since in the partition function configuration integral, this is a set of measure zero. However, in a

finite-size simulation, the integral is replaced by a sum, and the incorrect description of the system arising from the linear dependence leads to an  $\mathcal{O}(\frac{1}{N})$  error. If transformation properties consistent with our symmetry criterion are chosen and the normalization requirement imposed, these finite-size simulation errors and the unnecessary complications in the first-principles fitting procedure are avoided.

#### IV. EFFECTIVE HAMILTONIANS FOR CUBIC SYSTEMS

In this section, we generalize the construction of the effective Hamiltonian to arbitrary structures and apply it to phonon-related structural transitions in the perovskite, rocksalt, fluorite and A15 structures. We will use as our primary illustration the example of the perovskite structure. Among the many compounds in this structure, a rich variety of phonon-related structural transitions are found.<sup>9</sup> These can be analyzed in a unified systematic framework using the present approach.

The cubic perovskite structure, which will be taken as the high-symmetry reference structure, has five atoms per unit cell and space group  $Pm3m$ . The first step in the effective Hamiltonian construction is a symmetry analysis to identify the band subspaces (i.e. minimal invariant subspaces spanned by one or more entire branches of normal modes). Once the space group irrep labels for the ionic-displacement space have been determined, a complete list of the band subspaces and the corresponding Wannier basis labels can be obtained by the following general procedure, valid for arbitrary structures. First, all possible symmetry types of band subspaces are constructed using the compatibility relations between the irrep labels at the high-symmetry  $\vec{k}$ -points. The corresponding Wannier basis labels are found by considering in turn each Wyckoff symbol with each irreducible representation of the corresponding site symmetry group such that the product of the number of the Wyckoff positions with the dimension of the site symmetry group irrep is less than or equal to the maximum multiplicity of the band subspaces. A particular combination will label a Wannier basis of a band subspace if the space group irrep labels produced at the high-symmetry  $\vec{k}$ -points match

those of the band subspace.<sup>21</sup> Application of this procedure to the perovskite structure yields four band subspaces, all labelled by occupied Wyckoff positions with vector representations, corresponding to atomic displacements. These are listed in Table I.

As in the case of the diatomic chain, a parametrization of the displacement pattern of the Wannier basis vectors can be obtained from symmetry considerations. For each band subspace, the procedure is (1) choose one of the Wyckoff positions specified by the label; (2) identify the symmetric coordination shells surrounding that site; and (3) compute the independent displacement patterns of each shell that transform according to the given irreducible representation of the site symmetry group. For each of the four band subspaces of the perovskite structure, the displacement patterns for the innermost coordination shells are shown in Fig. 6. The relative amplitudes of each independent displacement pattern for each shell are free parameters determined by the requirement that a particular branch or branches of normal modes be reproduced, and thus will be different for individual materials.

As we have seen in Section II, construction of an effective Hamiltonian involves the choice of an invariant subspace as the direct sum of one or more band subspaces. The effective Hamiltonian subspace should include all modes relevant to the particular transition being modelled. The smallest subspace satisfying this condition, and therefore the maximum possible reduction in the degrees of freedom, can be identified by listing the symmetry labels of the relevant modes and choosing a direct sum of the band subspaces of the ionic-displacement space which produces the desired labels. There are cases in which there is more than one minimal choice which satisfies the conditions. If the choices differ in the other symmetry labels, the choice is made for an individual material by determining the symmetry labels of the lowest-energy modes at other high-symmetry  $\vec{k}$ -points. If all symmetry labels are the same, then the Berry phase label<sup>22,25</sup> determines the choice, since well-localized Wannier basis vectors are only obtained by transforming eigenvector branches which are smooth in  $\vec{k}$ . The general analysis of Berry phases for composite energy bands is quite complicated.<sup>26</sup> For present purposes, we observe that if only one of the possible choices is produced by an occupied Wyckoff position combined with a vector representation, that choice will smoothly

reproduce the physical eigenvector branch. Examples of systems where more than one choice is of this kind can be constructed, the simplest being a crystal of space group  $F222$  ( $\# 22$ )<sup>27</sup> with both the 2a and 2b Wyckoff positions occupied. In such cases, it is advisable to include both branches in the effective Hamiltonian subspace, with two Wannier basis vectors, one centered on each Wyckoff position. Only if the “relevant phonon” is heavily dominated by displacements of only one of the two atom types should construction of a subspace with only one Wannier basis vector (centered on the corresponding Wyckoff position) be considered. In the crystal structures analyzed in this section, this difficulty does not arise.

With the selection of the effective Hamiltonian subspace, the invariant expansion of the lattice energy in Wannier basis coordinates proceeds straightforwardly, facilitated by the symmetry properties of the Wannier basis vectors. Different structural transitions observed in perovskite structure compounds require different treatment, starting at this point. In the following, we will consider four common perovskite transitions (i) the ferroelectric transition in  $BaTiO_3$  and  $PbTiO_3$ , with an unstable  $\Gamma_{15}$  mode; (ii) the oxygen-octahedron rotational transition in  $SrTiO_3$ , with an unstable  $R_{25}$  mode; (iii) the Jahn-Teller instability in  $La_{1-x}(Ca, Sr, Ba)_xMnO_3$ , with an unstable  $R'_2$  mode; and (iv) the antiferroelectric transition in  $PbZrO_3$ , involving several unstable modes.

For the  $\Gamma_{15}$  ferroelectric transition found in  $BaTiO_3$  and  $PbTiO_3$ , all four subspace choices  $A$ ,  $B$ ,  $O_{x,x}$  and  $O_{x,y}$  are consistent with the symmetry criterion. The simplest form of the effective Hamiltonian is obtained by choosing either the  $3N$ -dimensional subspace  $A$ , resulting in the invariant energy expansion for  $PbTiO_3$  of Ref. 5, or the  $3N$ -dimensional subspace  $B$  for  $BaTiO_3$  as in Ref. 6. In these two cases, the choice of  $A$  versus  $B$  is determined by the symmetry labels of the lowest zone-boundary modes. In these systems, coupling to strain is known to be important.<sup>5,28,29</sup> Homogeneous strain is easily included by introducing the six-component strain variable  $e_{\alpha\beta}$  ( $\alpha, \beta = x, y, z$ ) and its lowest order coupling to the ferroelectric mode coordinates.<sup>4-6</sup> To include inhomogeneous strain as well, the subspace can be enlarged by adding a second band subspace containing  $\Gamma_{15}$  to describe the acoustic modes. The most convenient choice is the cation subspace not already used

for the ferroelectric mode. In addition to the space group symmetries, the inhomogeneous strain Hamiltonian has global translation and rotation invariances which can most easily be satisfied by following the construction method of Keating.<sup>30</sup> If the expansion is truncated at three independent parameters, corresponding to the three elastic constants, the strain Hamiltonian used in Ref. 6 is obtained. Additional expansion parameters could be included to improve the description of the acoustic modes away from the zone center. With Wannier basis vectors that exactly reproduce the mode eigenvectors, there is no quadratic coupling between the two subspaces  $A$  and  $B$ . The lowest order anharmonic coupling that does not vanish in the limit  $\vec{k} \rightarrow 0$  is the coupling term used in Ref. 6.

The  $R_{25}$  oxygen-octahedron rotational transition occurs in  $SrTiO_3$  at 105 K and in a number of other systems.<sup>31</sup> This unstable mode is built up in Refs. 2 and 7 from a Wannier-like “rotational variable” transforming according to  $T_{1g}$ <sup>32</sup> at each site of the simple cubic lattice. Symmetry analysis shows that this basis set is linearly dependent, generating symmetry labels  $\Gamma'_{25}$ ,  $\Delta'_2$  and  $X_2$  which do not appear in the symmetry decomposition of the ionic displacement space. While this difficulty can be formally resolved by requiring the energy to be zero for configurations with  $\vec{k}$  in  $\Gamma - \Delta - X$ , the vanishing of the normalization at lines in the Brillouin zone leads to  $\mathcal{O}(\frac{1}{N^2})$  errors in finite-size simulations, as discussed in the previous section for the diatomic chain. Also, incorporation into the effective Hamiltonian of first-principles results at these lines requires extra manipulations. Finally, use of this basis in quantum-mechanical or dynamical studies, in which the kinetic energy must be treated explicitly, would complicate the analysis by introducing an artificially vanishing effective mass in the neighborhood of these lines.

In the present approach, to describe the  $R_{25}$  oxygen-octahedron rotational transition in  $SrTiO_3$ , the band subspace is the  $6N$  dimensional space  $O_{x,y}$ . The resulting effective Hamiltonian describes a system of two-component vectors on the faces of the unit cells of the simple cubic lattice (Fig. 7(a)). This form is slightly more complicated than the models usually studied in the statistical mechanics literature, since the “spin” sites do not form a Bravais lattice. However, symmetry still ensures that the invariant energy expansion is

fairly simple. In fact, the quadratic part has the form of a submatrix of the familiar force constant matrix for the perovskite structure. Furthermore, this form presents no problems for numerical analysis of the model through Monte Carlo simulation. Even the fact that the band subspace is six dimensional can be turned to advantage. The extra  $\Gamma_{15}$  mode can be used to describe inhomogeneous strain coupling or the ferroelectric mode, which is observed to be nearly unstable.<sup>33</sup>

To describe the  $R'_2$  Jahn-Teller instability in  $La_{1-x}(Ca, Sr, Ba)_xMnO_3$ <sup>34</sup> the invariant subspace for effective Hamiltonian construction must include the  $3N$  dimensional band subspace labelled  $O_{x,x}$  in Table I. The resulting effective Hamiltonian describes a system of one-component vectors on the edges of the unit cells of a simple cubic lattice. As in the case of  $SrTiO_3$ , the invariant energy expansion turns out to be simple and quite tractable for analysis through Monte Carlo simulation. The symmetry of the model can also be readily exploited in writing the form of the coupling to electronic states.<sup>8</sup>

For antiferroelectric  $PbZrO_3$ , there are four relevant modes: an  $R_{25}$  oxygen-octahedron rotation, a  $\Gamma_{15}$  polar mode, a  $(\frac{1}{2}\frac{1}{2}0)(\frac{\pi}{a})\Sigma_3$  mode, and a  $(110)(\frac{\pi}{a})M'_5$  mode.<sup>35</sup> All these modes are included in the  $6N$ -dimensional band subspace  $O_{x,y}$  (Fig. 7(a)), so that the resulting effective Hamiltonian is surprisingly simple for such a complex transition. To examine the effects of coupling to inhomogeneous strain, the effective Hamiltonian subspace would have to be extended to include an additional  $3N$ -dimensional subspace ( $A$  or  $B$ ).

The analysis for structural transitions occurring in other structures proceeds similarly. The rocksalt-rhombohedral transition in  $GeTe$  has been previously studied with a first-principles model Hamiltonian approach.<sup>4</sup> The high-symmetry reference structure is the rocksalt structure, with an  $fcc$  Bravais lattice with conventional lattice constant  $a_0$  and space group  $Fm3m$ . The symmetry analysis of the band subspaces is given in Table II. The soft mode of the transition to the rhombohedral structure is  $\Gamma_{15}$ , so both  $Ge$  and  $Te$  are possible choices for the effective Hamiltonian subspace. As in the perovskite structure, the choice is determined by the symmetry label of the lowest energy zone-boundary mode. The effective Hamiltonian constructed with the  $Te$  subspace is a system of three-component spins on an

*fcc* lattice of lattice constant  $a_0$ . In Ref. 4, coupling to homogeneous strain was included and good agreement obtained with the experimental transition behavior. The rocksalt structure is so simple that if inhomogeneous strain were included in the model (by adding the *Ge* subspace) the resulting “effective Hamiltonian” subspace would be the full ionic displacement space, and the effective Hamiltonian would be identical to  $\mathcal{H}_{lat}$ .

The cubic-tetragonal transition in  $ZrO_2$  has inspired several recent first-principles band-structure and total-energy studies.<sup>37</sup> In this system, the high-symmetry reference structure is the fluorite structure, with an *fcc* Bravais lattice with conventional lattice constant  $a_0$  and space group  $Fm\bar{3}m$ . The symmetry analysis of the band subspaces is given in Table III. The soft mode of the transition to the tetragonal structure is  $X'_2$ , so the effective Hamiltonian subspace must be the  $6N$ -dimensional space  $O$ . The resulting effective Hamiltonian is a system of three-component spins on a simple cubic lattice of lattice constant  $\frac{a_0}{2}$ . However, the symmetry for the invariant energy expansion is not  $O_h$ , but  $T_d$ , imposed by the presence of the *fcc* zirconium sublattice.

Structural transitions in A15 compounds such as  $V_3Si$  have long been of interest because of the interplay with “high-temperature” superconductivity in these systems.<sup>38</sup> The A15 structure has two formula units (8 atoms) per unit cell, with a simple cubic Bravais lattice and a nonsymmorphic space group  $Pm\bar{3}n$ . The symmetry analysis of the band subspaces is given in Table IV. The observed low-temperature structure is generated by the  $\Gamma_{12}$  mode. The effective Hamiltonian subspace is then the  $6N$ -dimensional space  $A_{||}$ . The choice of  $A_{||}$  over  $6d, \vec{u}_{||}$ , which also produces the right symmetry label, is made on the basis of the Berry phase argument discussed earlier in this section. The resulting model is a system of one-component vectors on three interpenetrating sets of chains running along the cartesian directions. The  $\Gamma_{15}$  mode in this subspace can be used to include the effects of coupling to inhomogeneous strain.

## V. PRACTICAL ASPECTS OF FIRST-PRINCIPLES IMPLEMENTATION

The information available from first-principles methods is (i) total energy of supercells; and (ii) force constant matrices at various  $\vec{k}$  calculated using density functional theory linear response.<sup>15–18</sup> In this section, we present a practical approach for using this information to construct the effective Hamiltonian for a particular system, illustrating the procedure with the application to the ferroelectric transition in  $PbTiO_3$ .<sup>5</sup>

The analysis begins with the identification of the high-symmetry reference structure and relevant phonon, and the first-principles calculation of the force constant matrices (either by linear response or by frozen phonon supercell calculations) at the high-symmetry  $\vec{k}$ -points. The first step is to identify the effective Hamiltonian subspace  $\Lambda_0$ . For some structural transitions,  $\Lambda_0$  will be a single band subspace uniquely specified by the relevant phonon. For others, the relevant phonon allows a choice of band subspaces. In the example of the  $PbTiO_3$  transition, the  $\Gamma_{15}$  phonon allows a choice of band subspaces  $A$ ,  $B$ ,  $O_{x,x}$  and  $O_{x,y}$ . The choice should be made so as to include the lowest energy eigenmodes at other high-symmetry  $\vec{k}$ -points. In  $PbTiO_3$ , the low energy modes  $X'_5$ ,  $M'_2$ ,  $M'_5$ , and  $R_{15}$  determine the effective Hamiltonian subspace to be the band subspace  $A$  (see Table I).

The next step is the construction of the Wannier basis vectors for the subspace  $\Lambda_0$ . The strategy is to fit independent displacement parameters for the innermost coordination shells to the normalized eigenvectors at only the high-symmetry  $\vec{k}$ -points (with adjustment of the eigenvector phases to obtain optimally rapid decay). Since the Wannier basis vector ionic displacements generally decay rather rapidly with distance from the central ion, this is sufficient to determine an excellent approximation to the Wannier basis vector. In the example of the diatomic chain, discussed in Section III, it was sufficient to fit only the  $k = 0$  and  $k = \pi$  modes. The application to ionic insulating crystals, including  $PbTiO_3$ , requires additional comment. If  $\Lambda_0$  contains a degenerate polar  $k = 0$  mode and there are polar  $k = 0$  modes not included in  $\Lambda_0$ , (as, for example, in the perovskite structure<sup>40</sup>), the electric field at  $k \rightarrow 0$  mixes the LO modes differently from the TO modes, and a single Wannier basis vector

cannot faithfully reproduce both the transverse and longitudinal branches. Therefore, the normal modes of the corresponding longitudinal branch should *not* be used in constructing the approximate Wannier basis vector. The correct approach is to use only the low energy (transverse) branches to determine the approximate Wannier basis vector. For  $PbTiO_3$ , we use displacements of the central, first and second neighbor Pb ions and the nearest Ti and O shells, for a total of nine independent parameters (six of which are included in Fig. 6) to reproduce the normalized lowest-frequency normal modes  $\Gamma_{15}$ ,  $R_{15}$  and  $M'_2$  and the normalization of the  $M'_5$  mode exactly. The amplitudes of the displacements are found to decay rapidly, as expected. Moreover, the  $X'_5$  and  $M'_5$  normal modes predicted from the parameters obtained from the fit are in excellent agreement with the corresponding normalized normal modes calculated from first principles.<sup>5</sup>

The form of the effective Hamiltonian is obtained by Taylor expanding the potential energy in symmetry invariant combinations of the  $\xi_i$  and approximating to obtain an expression with a relatively small number of effective Hamiltonian parameters which can be determined from the available information. For the quadratic part of the effective Hamiltonian, this will mean that intercell interactions of the most general form are included only up to a finite range. For  $PbTiO_3$ , we include general intercell interactions up to third neighbor (eight independent parameters). The long-range dipolar interactions required for the correct description of polar modes can be included in a parametrized form, requiring only knowledge of the Born effective charges  $Z^*$  and the dielectric constant  $\epsilon_\infty$ , which can be obtained from separate linear response calculations or from energies of distortions with  $\vec{q}$  close to zero. Similarly, a small number of higher order terms must be selected so as to ensure stability and a ground state configuration of the correct type. In  $PbTiO_3$ , only onsite anharmonic terms are needed. Lastly, in a cubic system such as  $PbTiO_3$ , inclusion of the coupling to homogeneous strain introduces only a few additional parameters.

The calculation of the parameters in the effective Hamiltonian exploits the fact that a given set of Wannier basis coordinates uniquely determines the positions of the ions. The quadratic parameters are obtained by fitting to the frequencies of a set of modes in the ef-

fective Hamiltonian subspace computed from first-principles force-constant matrices at the high-symmetry points  $\vec{k}$ -points and at  $\vec{k}$ -points along selected symmetry lines. In  $PbTiO_3$ , we compute  $Z^*$  and  $\epsilon_\infty$  from DFT perturbation theory, and fit the eight short-range interaction parameters to the following effective Hamiltonian eigenmodes:  $\{\Gamma_{15}, R_{15}, M'_2, M'_5, X'_2, X'_5\}$  and the  $\Lambda_3$  modes at  $\frac{\pi}{2a_0}(111)$  and  $\frac{\pi}{4a_0}(111)$ . The truncations in the Taylor expansion of the quadratic effective Hamiltonian can be checked by computing force constant matrices at additional  $\vec{k}$ . With linear response, this overdetermination of parameters is relatively easy, while it can be quite impractical in supercell calculations. In the same way, anharmonic terms can be obtained from fitting the higher-order dependence of first-principles total energies on the amplitude of the Wannier basis coordinates. Lastly, the homogeneous strain terms are obtained by computing the dependence of total energies of configurations on variations in the lattice parameters.

The approximate Wannier basis vector approach can be applied successfully even if the branches of interest are not fully isolated in energy from other branches, which are recognizable by distinct symmetry labels. Even in this case, a simple model, with the effective Hamiltonian acting in the  $\Lambda_0$  subspace, should still give accurate results for finite-temperature properties if the  $\Lambda \neq \Lambda_0$  branches cross only the higher-energy portions of the  $\Lambda_0$  branches, preferably at  $\vec{k}$ -points far from the  $\vec{k}$  of the relevant phonon. In that case, the approximate Wannier basis vector is fit using only the normalized eigenvectors at  $\vec{k}$ -points where the  $\Lambda_0$  branches can be distinguished from the  $\Lambda \neq \Lambda_0$  branches by their symmetry labels. This set of  $\vec{k}$ -points will typically be the same as the set of high-symmetry  $\vec{k}$ -points prescribed in the general procedure for approximate Wannier basis vector construction. Similarly, at other  $\vec{k}$ -points, energies of the approximate eigenvectors built up from these approximate Wannier basis vectors are computed from force constant matrix results and used to determine effective Hamiltonian parameters. Therefore, application of the approximate Wannier basis vector approach essentially projects out the  $\Lambda \neq \Lambda_0$  character at the low-symmetry  $\vec{k}$ -points, which amounts to ignoring the crossing.

If a substantial amount of crossing occurs into the lower energy range, if all the relevant

modes are not contained in a single band subspace, or if anharmonic coupling to modes outside the relevant band subspace is important, it will be necessary to enlarge the effective Hamiltonian subspace to include the additional branches by working with a direct sum  $\Lambda_1 \oplus \Lambda_2 \oplus \dots \oplus \Lambda_s$ . For each band subspace, there is an independent Wannier basis vector to be determined by fitting eigenvector information. If the approximate Wannier basis vectors exactly reproduce all branches at all calculated  $\vec{k}$ -points, then in the invariant energy expansion there are no cross terms between coordinates from different band subspaces. If this is not the case (for example, for the polar modes discussed above) cross terms must be included in the invariant energy expansion and explicitly determined from the force constant matrix information.

If the subspace containing the relevant modes contains no polar modes and is well separated in energy from the higher-energy eigenmodes, there is an alternative approach which bypasses the explicit construction of the Wannier basis vectors altogether by applying the philosophy of tight-binding parameterization of electronic energy bands.<sup>41</sup> In that case, we assume the existence of underlying Wannier basis vectors and fit directly to the eigenvalues to obtain effective Hamiltonian parameters. This approach was discussed in Section III for the diatomic chain example, which satisfies the necessary conditions. In applications to real materials, this ideally simple situation is not expected to be very common, and therefore the approximate Wannier basis vector construction is recommended for routine use.

## VI. CONCLUSIONS

A systematic procedure has been presented for the construction of localized Wannier basis vectors and corresponding effective Hamiltonians, applicable to arbitrary structures and phonon-related transitions. The application to several different structures has been described. For the perovskite structure, a new approach to the oxygen-octahedron transition in  $SrTiO_3$  is suggested, which avoids the subtle difficulties arising from the use of a “rotational variable.” Improvements can be systematically made by including additional

band subspaces in the effective Hamiltonian subspace, if indicated by the presence of substantial crossing of eigenmode branches or strong anharmonic coupling to inhomogeneous strain or other modes. The effective Hamiltonian parameters for a particular material can be obtained using any method that can reliably calculate force constants and distortion energies. Once the force-constant matrices have been calculated, the construction of an effective Hamiltonian is straightforward and requires very little additional computational effort. An efficient method, such as DFT linear-response, expedites the necessary overdetermination of effective Hamiltonian parameters. Further applications of this approach could include the construction of realistic quantum mechanical models for the study of quantum paraelectrics and ferroelectrics,<sup>42</sup> as well as classical dynamical models for the study of ferroelectric phenomena such as switching. In addition, these effective Hamiltonians can be used for realistic first-principles studies of thermal expansion and other temperature dependent lattice properties,<sup>43</sup> as well as for structural transitions. More generally, the construction of a Wannier basis may prove advantageous for the treatment of localized perturbations.

### Acknowledgments

We thank R. B. Phillips, G. Moore, S. Ogut, A. J. Millis, A. Rappe and W. Zhong for useful discussions. We thank D. Vanderbilt, H. T. Stokes, and D. M. Hatch for useful discussions and for valuable comments on the manuscript. This work was supported by ONR Grant N00014-91-J-1247. In addition, K. M. R. is grateful for the hospitality of l'Ecole d'Eté de Physique Théorique Les Houches during part of this work, and for the support of the Clare Boothe Luce Fund and the Alfred P. Sloan Foundation.

## REFERENCES

- <sup>1</sup> H. Thomas and K. A. Muller, Phys. Rev. Lett. **21**, 1256 (1968).
- <sup>2</sup> E. Pytte, Phys. Rev. **B5**, 3758 (1972); E. Pytte and J. Feder, Phys. Rev. **187**, 1077 (1969); J. Feder and E. Pytte, Phys. Rev. **B1**, 4803 (1970).
- <sup>3</sup> M. E. Lines, Phys. Rev. **177**, 797 (1969).
- <sup>4</sup> K. M. Rabe and J. D. Joannopoulos, Phys. Rev. Lett. **59**, 570 (1987); Phys. Rev. **B36**, 6631 (1987); in *Electronic Phase Transitions*, ed. by W. Hanke and Y. V. Kopaev (North-Holland, Amsterdam, 1992), Chap. 3.
- <sup>5</sup> K. M. Rabe and U. V. Waghmare, Ferroelectrics **151**, 59 (1994); Ferroelectrics **164**, 15 (1995); unpublished.
- <sup>6</sup> W. Zhong, D. Vanderbilt and K. M. Rabe, Phys. Rev. Lett. **73**, 1861 (1994).
- <sup>7</sup> W. Zhong and D. Vanderbilt, Phys. Rev. Lett. **74**, 2587 (1995).
- <sup>8</sup> P. B. Littlewood, A. J. Millis and B. I. Shraiman, unpublished.
- <sup>9</sup> B. Lüthi and W. Rehwald, in *Structural Phase Transitions I*, ed. by K. A. Müller and H. Thomas, (Springer, 1981), Chap. 4.
- <sup>10</sup> L. D. Landau and E. M. Lifshitz, *Statistical Physics*, (Pergamon, 1963).
- <sup>11</sup> W. Kohn, Phys. Rev. **B7**, 2285 (1973).
- <sup>12</sup> J. C. M. Tindemans-van Eijndhoven and C. J. Kroese, J. Phys. C **8**, 3963 (1975).
- <sup>13</sup> W. Kohn, Phys. Rev. **115**, 809 (1959).
- <sup>14</sup> J. des Cloizeaux, Phys. Rev. **135**, A698 (1964).
- <sup>15</sup> S. Baroni, P. Giannozzi and A. Testa, Phys. Rev. Lett. **58**, 1861 (1987).
- <sup>16</sup> X. Gonze, D. C. Allan and M. P. Teter, Phys. Rev. Lett. **68**, 3603 (1992).

- <sup>17</sup> U. V. Waghmare, V. Milman and K. M. Rabe, unpublished.
- <sup>18</sup> C. Z. Wang, R. Yu and H. Krakauer, Phys. Rev. Lett. **72**, 368 (1994); R. Yu and H. Krakauer, Phys. Rev. **B49**, 4467 (1994).
- <sup>19</sup> D. M. Hatch, H. T. Stokes and R. M. Putnam, Phys. Rev. **B35**, 4935 (1987).
- <sup>20</sup> H. T. Stokes, D. M. Hatch and J. D. Wells, Phys. Rev. **B43**, 11010 (1991).
- <sup>21</sup> The tedium of generating these tables for a complicated crystal structure can be relieved through the use of the computer program ISOTROPY, described in H. T. Stokes, Ferroelectrics (in press).
- <sup>22</sup> L. Michel and J. Zak, Europhys. Lett. **18**, 239 (1992).
- <sup>23</sup> R. A. Cowley, Phys. Rev. **134A**, 981 (1964).
- <sup>24</sup> G. F. Koster, *Solid State Physics*, edited by F. Seitz and D. Turnbull (Academic, 1957), Vol. 5.
- <sup>25</sup> M. B. Walker and J. Zak, Europhys. Lett. **26**, 481 (1994).
- <sup>26</sup> J. Zak, unpublished.
- <sup>27</sup> H. Bacry, L. Michel and J. Zak, Phys. Rev. Lett. **61**, 1005 (1988).
- <sup>28</sup> R. E. Cohen and H. Krakauer, Ferroelectrics **136**, 65 (1992); R. E. Cohen, Nature **358**, 136 (1992).
- <sup>29</sup> R. D. King-Smith and D. Vanderbilt, Phys. Rev. **B49**, 5828 (1994).
- <sup>30</sup> P. N. Keating, Phys. Rev. **145**, 637 (1966).
- <sup>31</sup> M. E. Lines and A. M. Glass, *Principles and Applications of Ferroelectrics and Related Materials* (Oxford, 1977), Chap. 8.2.1.
- <sup>32</sup> G. Burns, *Introduction to Group Theory with Applications*, (Academic, 1977), p. 388.

- <sup>33</sup> Ref. 31, Chap. 8.1.7.
- <sup>34</sup> J. B. Goodenough, Phys. Rev. **100**, 564 (1955); J. Kanamori, J. App. Phys. **31**, 14S (1960).
- <sup>35</sup> W. Cochran and A. Zia, Phys. Stat. Sol. **25**, 273 (1968).
- <sup>36</sup> L. P. Bouckaert, R. Smoluchowski and E. Wigner, Phys. Rev. **50**, 58 (1936).
- <sup>37</sup> R. E. Cohen, M. J. Mehl, and L. L. Boyer, Physica B+C **150**, 1 (1988); H. J. F. Jansen, Phys. Rev. **B43**, 7267 (1991); R. Orlando, C. Pisani, C. Roetti and E. Stefanovich, Phys. Rev. **B45**, 592 (1992); E. H. Sevilla and G. W. Fernando, unpublished.
- <sup>38</sup> J. F. Scott, Rev. Mod. Phys. **46**, 83 (1974).
- <sup>39</sup> W. Gorzkowski, Phys. Stat. Solidi **3**, 910 (1963).
- <sup>40</sup> W. Zhong, R. D. King-Smith and D. Vanderbilt, Phys. Rev. Lett. **72**, 3618 (1994).
- <sup>41</sup> J. C. Slater and G. F. Koster, Phys. Rev. **94**, 1498 (1954); W. A. Harrison, *Electronic Structure and the Properties of Solids*, (Freeman, San Francisco, 1980).
- <sup>42</sup> R. Martonak and E. Tosatti, Phys. Rev. **B49**, 12596 (1994).
- <sup>43</sup> O. Sugino and R. Car, unpublished.

TABLES

TABLE I. Band subspaces of the ionic displacement space of the perovskite structure. Subspaces are labelled by the corresponding Wyckoff symbol and site symmetry group irrep. In cases where the subspace is generated by a set of occupied Wyckoff positions and a vector representation, the atom type is used as the label. For each subspace, the symmetry labels at the high-symmetry  $\vec{k}$ -points are as in Ref. 23, with conventions taken from Ref. 24 and origin at A.

|           | $\Gamma$                   | $R$              | $X$                   | $M$                   |
|-----------|----------------------------|------------------|-----------------------|-----------------------|
| $A$       | $\Gamma_{15}$              | $R_{15}$         | $X'_2, X'_5$          | $M'_2, M'_5$          |
| $B$       | $\Gamma_{15}$              | $R'_{25}$        | $X_1, X_5$            | $M'_3, M'_5$          |
| $O_{x,x}$ | $\Gamma_{15}$              | $R'_2, R'_{12}$  | $X'_2, X_5$           | $M_2, M'_3, M_4$      |
| $O_{x,y}$ | $\Gamma_{15}, \Gamma_{25}$ | $R_{25}, R_{15}$ | $X_1, X_3, X_5, X'_5$ | $M_1, M_3, M_5, M'_5$ |

TABLE II. Band subspaces of the ionic displacement space of the  $GeTe$  rocksalt structure, as in Table I. Symmetry label conventions are taken from Ref. 36, with the origin at Te.

|      | $\Gamma$      | $L$          | $X$          | $W$          |
|------|---------------|--------------|--------------|--------------|
| $Ge$ | $\Gamma_{15}$ | $L_1, L_3$   | $X'_4, X'_5$ | $W_1, W_3$   |
| $Te$ | $\Gamma_{15}$ | $L'_2, L'_3$ | $X'_4, X'_5$ | $W'_2, W'_3$ |

TABLE III. Band subspaces of the ionic displacement space of the  $ZrO_2$  fluorite structure, as in Table I. Symmetry label conventions are taken from Ref. 36, with the origin at  $Zr$ .

|                   | $\Gamma$                    | $L$                    | $X$                    | $W$                         |
|-------------------|-----------------------------|------------------------|------------------------|-----------------------------|
| $Zr$              | $\Gamma_{15}$               | $L'_2, L'_3$           | $X'_4, X'_5$           | $W'_2, W_3$                 |
| $O$               | $\Gamma_{15}, \Gamma'_{25}$ | $L_1, L_3, L'_2, L'_3$ | $X_1, X_5, X'_2, X'_5$ | $W_1, W_3, W'_1, W_2, W'_2$ |
| $4b, \Gamma_{15}$ | $\Gamma_{15}$               | $L_1, L_3$             | $X'_4, X'_5$           | $W_1, W_3$                  |

TABLE IV. Band subspaces of the ionic displacement space of the A15 structure, as in Table I.  $A_{\parallel}$  denotes an A ion displacement along the chain direction and  $A_{\perp}$  denotes an A ion displacement perpendicular to the chain direction. For the  $6b$  sites, the irreducible representations of the site symmetry group are labelled by the component of a polar vector ( $\vec{u}$ ) or an axial vector  $\vec{R}$  parallel to the chain ( $\parallel$ ) or perpendicular and pointing along the direction to the nearest B atom ( $\perp, B$ ). For the  $6d$  sites, the polar vector components are parallel or perpendicular to the “chain” directions defined by these sites. Symmetry labels at  $\Gamma$  are taken from Ref. 36 and at zone boundary points from Ref. 39, with the origin at B.

|                           | $\Gamma$   | $R$     | $X$         | $M$               |
|---------------------------|--|---------|-------------|-------------------|
| $6c, A_{\parallel}$       | $\Gamma_2, \Gamma_{12}, \Gamma_{15}$                   | 4       | 1,1,3       | 1,2,5,8,9         |
| $6c, A_{\perp}$           | $\Gamma'_{15}, \Gamma_{15}, \Gamma'_{25}, \Gamma_{25}$ | 1,2,3,4 | 1,2,3,4,4,4 | 2,3,6,7,9,9,10,10 |
| $2a, B$                   | $\Gamma_{15}, \Gamma_{25}$                             | 4       | 1,3,4       | 1,2,5,6,10        |
| $6b, \vec{u}_{\parallel}$ | $\Gamma_{15}, \Gamma_{25}$                             | 4       | 1,3,3       | 2,3,6,7,9         |
| $6b, \vec{u}_{\perp, B}$  | $\Gamma_{15}, \Gamma_{25}$                             | 1,2,3   | 1,3,4       | 9,9,10            |
| $6b, \vec{R}_{\parallel}$ | $\Gamma'_{15}, \Gamma'_{25}$                           | 4       | 2,3,3       | 2,3,6,7,10        |
| $6b, \vec{R}_{\perp, B}$  | $\Gamma'_{15}, \Gamma'_{25}$                           | 1,2,3   | 2,3,4       | 9,10,10           |
| $6d, \vec{u}_{\parallel}$ | $\Gamma_2, \Gamma_{12}, \Gamma_{15}$                   | 4       | 1,1,3       | 1,2,5,8,9         |
| $6d, \vec{u}_{\perp}$     | $\Gamma'_{15}, \Gamma_{15}, \Gamma'_{25}, \Gamma_{25}$ | 1,2,3,4 | 1,2,3,4,4,4 | 2,3,6,7,9,9,10,10 |

## FIGURES

FIG. 1. The harmonic potential energy of the diatomic chain model is shown by two types of springs. One type, with spring constant  $\alpha$ , connects nearest neighbor A ions (open circles) and B ions (solid circles). The other, with spring constant  $\gamma$ , connects nearest neighbor B ions.

FIG. 2. Eigenvalues are shown as a function of  $k$  for the two branches of normal modes of the diatomic chain with  $\frac{\gamma}{\alpha} = 0.25$ . At  $k = 0$  and  $k = \pi$ , each branch is labelled by the appropriate irreducible representation of the space group and the corresponding displacement pattern is shown in the adjacent sketch. A ions are shown as open circles and B ions as solid circles.

FIG. 3. The harmonic potential energy of the triatomic chain model is shown by two types of springs. One type, with spring constant  $\alpha$ , connects nearest neighbor A ions (open circles) and B ions (solid circles). The other, with spring constant  $\gamma$ , connects nearest neighbor B ions.

FIG. 4. The displacement pattern of the Wannier function  $w_{\Lambda n}$ , corresponding to the lower branch in Fig. 2, is shown by the arrows. The pattern is odd around the central A ion. The arrows for the outermost A and B ions are smaller than the ion symbols.

FIG. 5. Dispersion  $\frac{\omega^2(k)}{S(k)}$  for the lower branch computed using the approximate Wannier function fit to  $k = 0$  (lower solid curve) compared with the true dispersion (dashed curve). The upper solid curve shows the overlap matrix element  $S$  as a function of  $k$ . For comparison, the upper dashed line is the unit normalization  $S = 1$ .

FIG. 6. Displacement patterns for the innermost coordination shells of representative Wannier basis vectors in each of the four band subspaces of the perovskite structure. The open squares represent the A ions, the shaded squares the B ions, and the open and shaded circles represent inequivalent oxygen ions. The four lines in the figure correspond to the subspaces A, B,  $O_{x,x}$  and  $O_{x,y}$ . In the first structure in each line, the displacement of each set of inequivalent ions can be specified independently.

FIG. 7. (a) The model system for the  $R_{25}$  oxygen-octahedron rotational transition in  $SrTiO_3$  consists of two-component vectors on the faces of the unit cell of a simple cubic lattice; (b) the model system for the  $R'_2$  Jahn-Teller instability in  $La_{1-x}(Ca, Sr, Ba)_xMnO_3$  consists of one-component vectors on the edges of the unit cells of a simple cubic lattice.

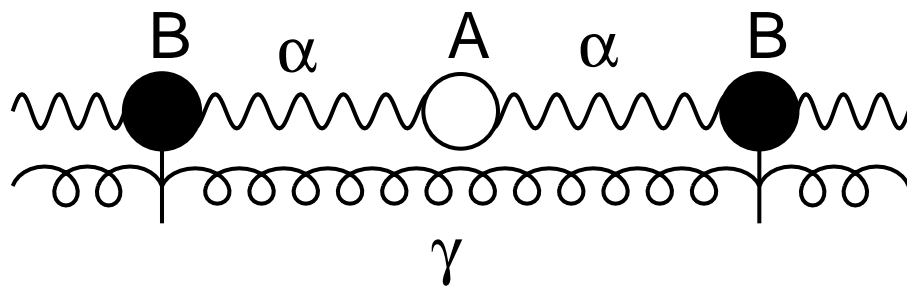
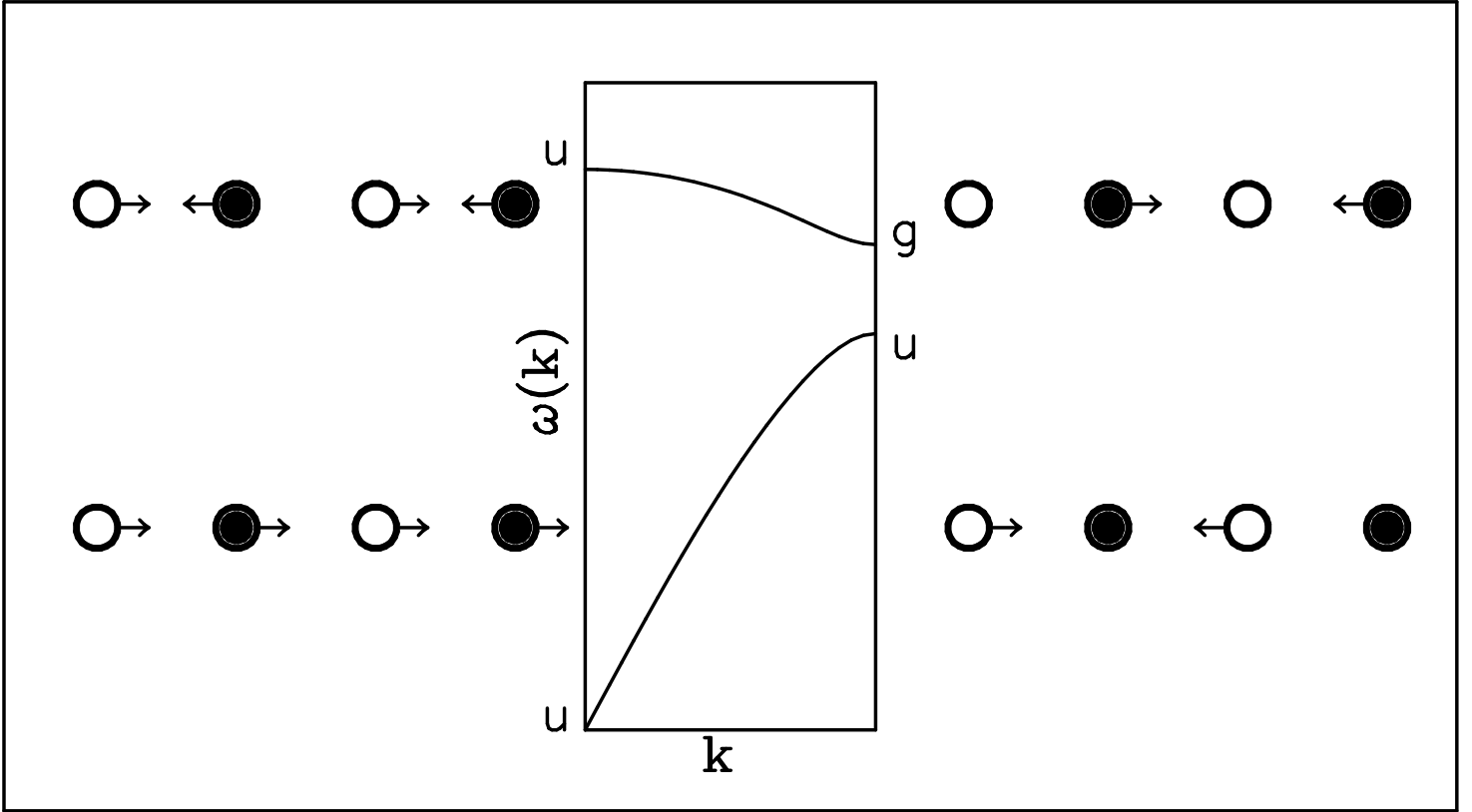


Figure 1



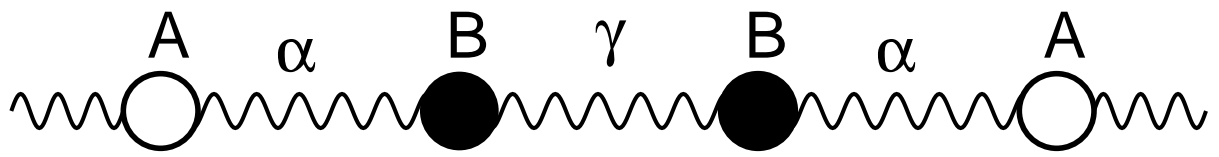


Figure 3

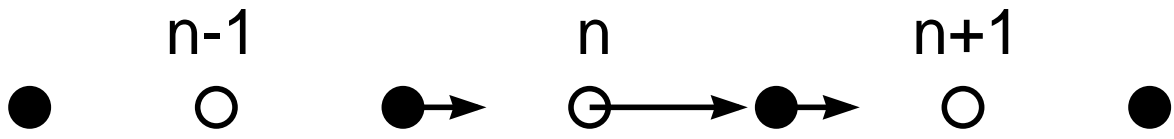
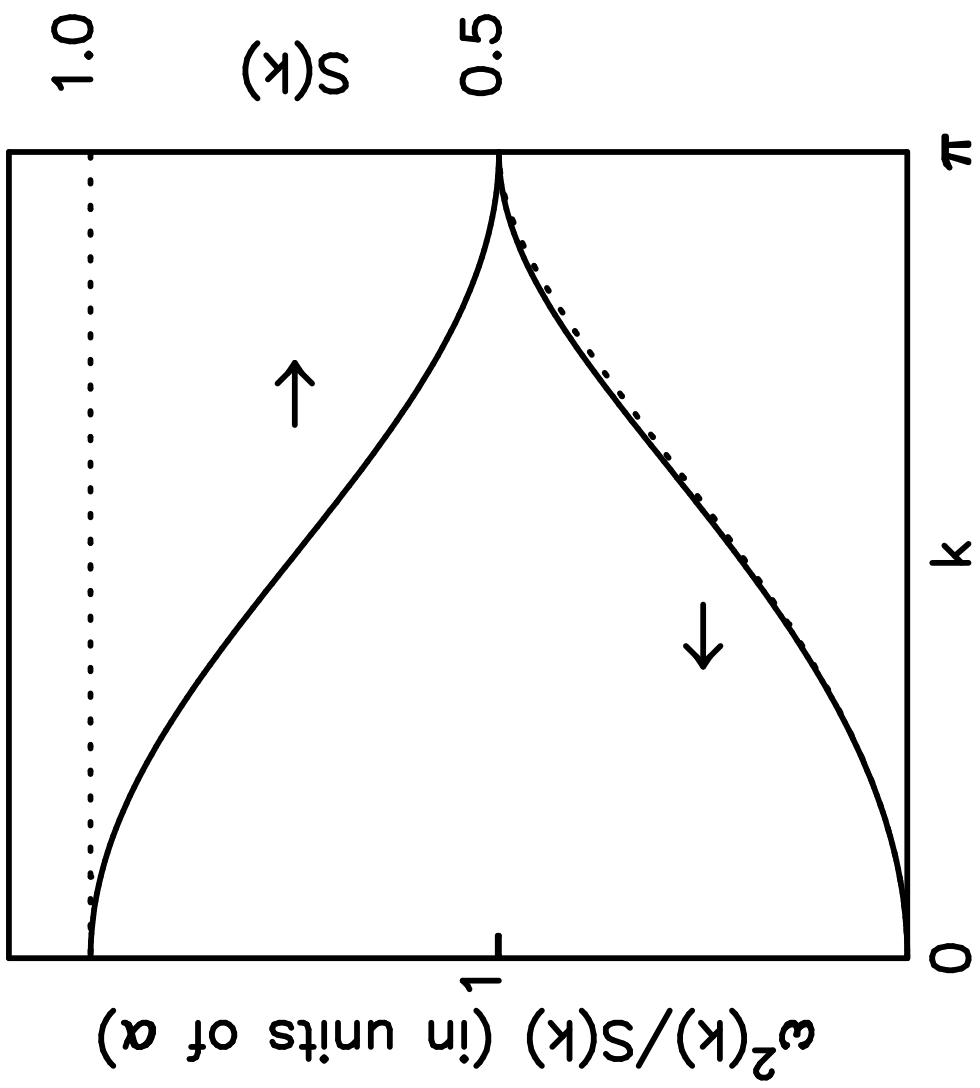
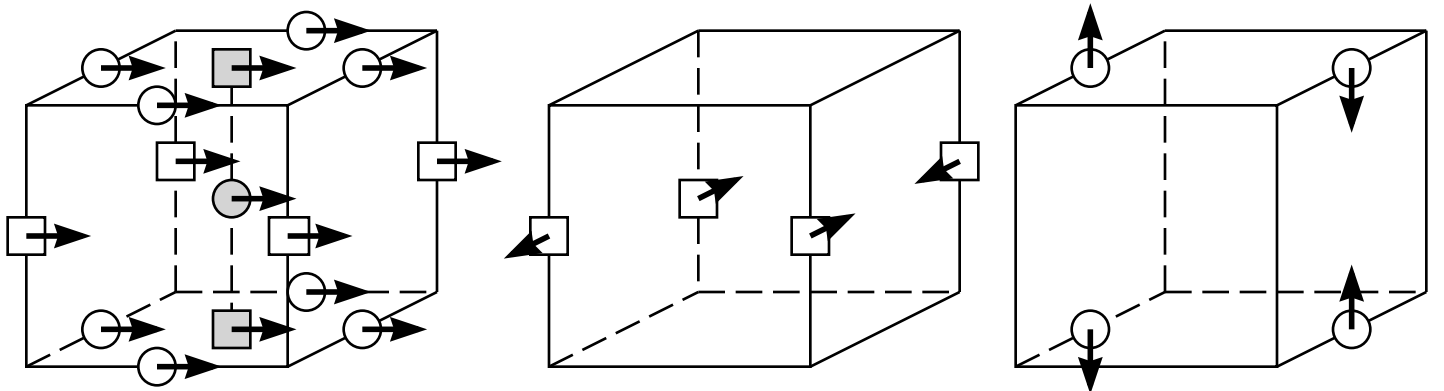
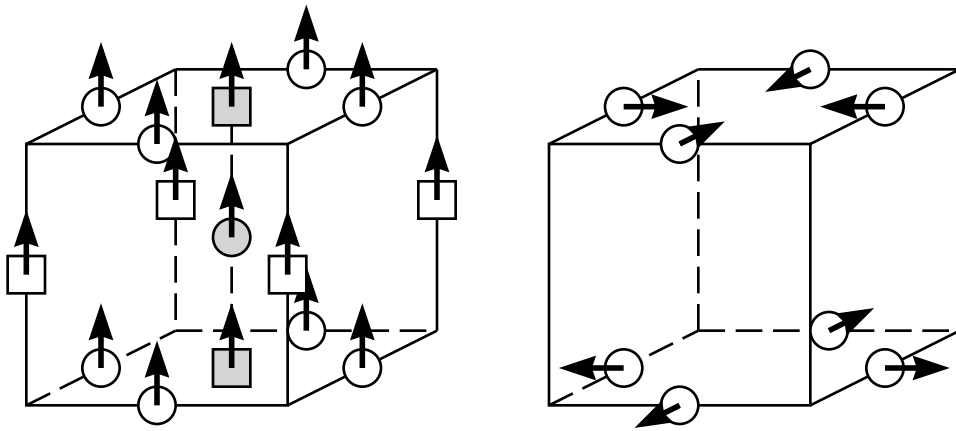
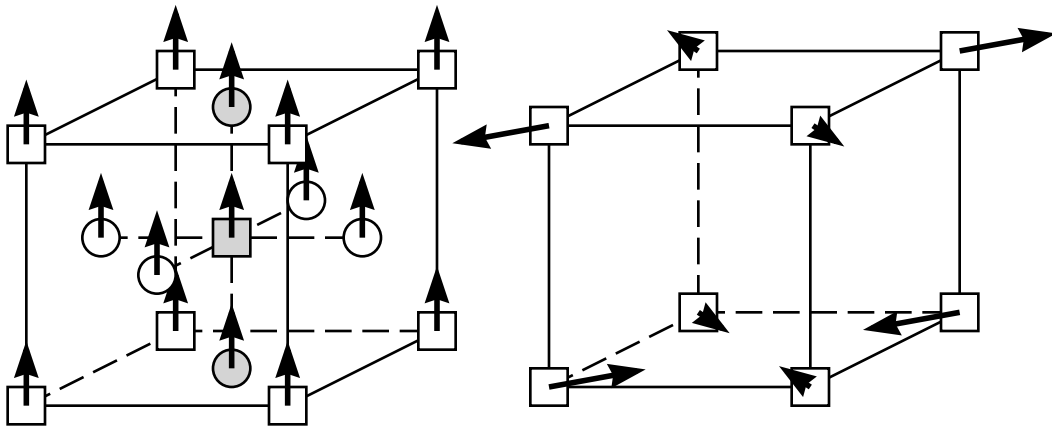
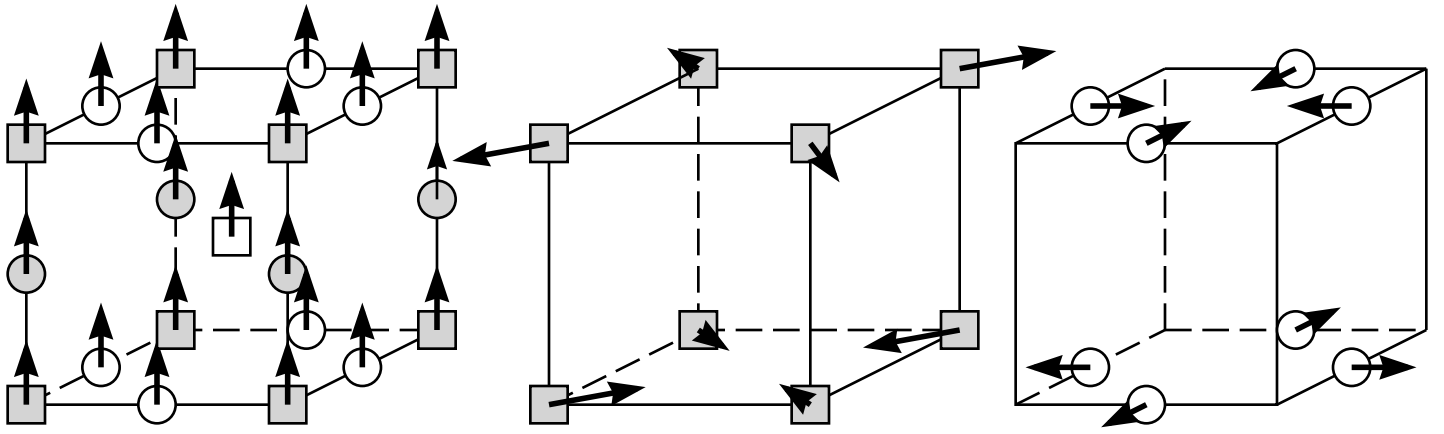
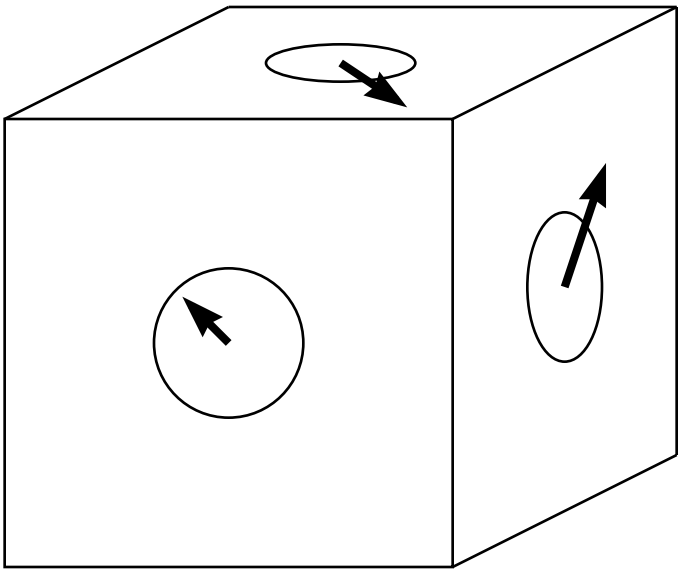


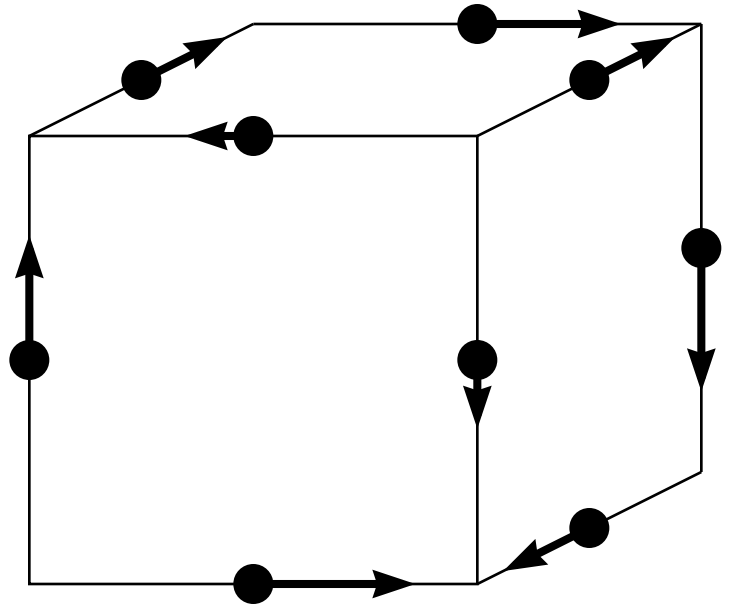
Figure 4







(a)



(b)

Figure 7